Development of a toolholder with high dynamic stiffness for mitigating chatter and improving machining efficiency in face milling

Yan Xia[1,2], Yi Wan[1, 2,*], Xichun Luo[3,*], Hongwei Wang[1,2], Ning Gong[4], Jinglong Cao[4], Zhanqiang Liu[1,2], Qinghua Song[1,2]

1. Key Laboratory of High Efficiency and Clean Manufacturing, School of Mechanical Engineering, Shandong University, Jinan, 250061, China

2. National Demonstration Center for Experimental Mechanical Engineering Education (Shandong University)

3. Centre for Precision Manufacturing, DMEM, University of Strathclyde, Glasgow, G1 1XJ, UK

4. Komatsu (Shan Dong) Construction Machinery Co., Ltd, Jining, 272073, China

Abstract:

The toolholder featuring large ratio of length to diameter and variable corss-sections is required to achieve some special machining tasks in face milling operation, whereas the chatter phenomenon can easily occur attributing to the weak dynamic characteristic of the toolholder. This paper developed a novel toolholder which possessed high dynamic performance and was able to mitigate the chatter and improve material removing rate (MRR) simultaneously. The relationship between dynamic property of cutter with its modal characteristics was theoretically investigated from the built dynamic model of face milling operation. Based on the above findings, a novel toolholder was designed to increase the dynamic stiffness of the cutter, whose geometrical parameters and corresponding materials were optimized and selected. After manufacturing and detecting, the stability and machining conditions of the new toolholder were validated and amended with the aid of transfer function, milling forces and acceleration signal responses obtained from the tool point dynamics test and milling experiments respectively. As demonstrated in the experimental results, comparing with the conventional toolholder, the dynamic stiffness of the developed toolholder was increased by about 3.75 times, expanding significantly the stability frontier. The corresponding MRR with 2.81 times was achieved without increasing the machining response amplitudes.

1. Introduction

Chatter is an unstable cutting state that may occur if the dynamic performance [1, 2] of the cutter [3] or workpiece [4] is poor or using wrong cutting parameters. The presence of severe chatter could produce harsh noise, degrade machined surface quality, accelerate tool wear and even catastrophic tool breakage which will reduce product quality and productivity. Milling vibration can be generally classified into two major categories, i.e. forced and self-excited vibrations [5]. As the most common self-excited vibration, the regenerative chatter has been widely investigated [6, 7]. Cutting parameters optimization, active and passive strategies are three major vibration control measures to avoid or attenuate chatter.

Cutting parameter optimization is to setup machining parameters which will allow the material removal taking place in a stable status to realize chatter-free milling. Two effective ways, known as stability lobe diagram (SLD) prediction and chatter detection, are usually used to select the right machining parameters. Merrit [8] proposed early that SLD is used to describe the relationship between spindle speed and the limit axial depth of cut during chatter-free milling. The milling dynamic models described the regeneration mechanism are always expressed in the form of the delay-differential equations, and the zero-order [9], multi frequency [10], semi-discrete [11,12] and full-discrete [13,14] methods are proposed in succession to calculate the SLD. Besides SLD prediction, the chatter detection is also used to identify the onset of chatter to maintain normal cutting. During machining process, responses signals, such as acceleration [15, 16], displacement [17], sound [2, 18] and cutting force [19], are

Nomenclature

ζ_γ $(\gamma = x, y, z)$	damping ratio of cutter in three orthogonal directions	N	number of tooth for cutter
k_γ	stiffness of cutter in three orthogonal directions	$a_{\lim}$	limit of axial depth of cut
$\omega_{n\gamma}$	natural frequency of cutter in three orthogonal directions	H_T, E_T	thickness and elasticity modulus of base body of toolholder
$F_{\gamma, j}$	cutting forces of insert j in three orthogonal directions	H_D, E_D	diameter and elasticity modulus of damping core
$F_{\mu, j}$ $(\mu = r, t, a)$	cutting forces of insert j in radial, tangential and axial directions	H_Y, E_Y	thickness and elasticity modulus of the inlaid strip
$K_{\mu c}, K_{\mu e}$	cutting coefficients and edge coefficients	δ_T, δ_D	micro deformations of toolholder substrate and damping core
ϕ_j	immersion angle	e	ratio E_D/E_T
κ	lead angle	h	ratio H_D/H_T
S	length of cutting edge of insert	ψ	angular displacement
A	time varying directional dynamic force coefficients	β	loss factor of damping material
$h(\varphi_j)$	instantaneous dynamic chip thickness	η	loss factor of toolholder
f_z	feed per tooth	MRR	material removing rate
Δt	vibration displacement of adjacent tooth	L	length of toolholder
$\Phi(i\omega)$	frequency response function	I	inertia moment
Ω	spindle speed	r_v	frequency ratio

collected and detected by sensors to monitor the process state. Although this category is able to avoid milling chatter and make milling process stable, it cannot improve the stability capacity of the milling system.

Unlike the strategy of cutting parameters optimization, the active and passive dynamic control technologies can expand the stability zone through modifying the dynamic behaviour of machining system [5] to improve MRR. Based on the feasibility, many active control devices have been designed. For instance, the active spindle systems with magnetic bearing [20] or piezoelectric actuator [21] are constructed to suppress the cutting chatter. The active clamping system for workpiece can also control the milling vibration by adjusting the relative position relationship between tool and workpiece [22]. Additionally, the milling stability limit is improved by the acceleration feedback system composed of sensor, control loop and machine drive [23]. To achieve the active control technique, however, it is essential to design the complex control device and provide extra energy, which will decrease the reliability and economy of the method and thus make it hard to apply in workshops.

In contrast to the active dynamic control method, it is easy to design and implement a passive technology from the aspect of industrial application [3]. The principle of this method is to increase dynamic characteristic of machining system to suppress or avoid the chatter. Various passive technology designs are proposed, such as tuned mass damper, frictional damper, constrained layer damper and material with high damping or rigidity. The research of tuned mass damper against chatter was initiated by Hahn [24], and extended by Kiran [25], Wan [26] and Yang [27, 28], et al. Frictional damper utilizes the friction force generated from the interaction between damper and vibration element to expend vibration energy [29]. According to the constrained layer damping mechanism [30], the damping ratio of tool can be improved and thereby vibration energy is dissipated. In addition, the material with high Young's modulus or damping can increase the stiffness or damping ratio of tool to enlarge the stable zone of SLD [1, 31].

The aforementioned literature dealt mainly with conventional milling cutter using the toolholder with constant cross-sectional diameter. To the best our knowledge, the chatter control of face milling cutter including a toolholder with large length-diameter ratio and variable cross-sections has not been studied yet. The milling

system may become unstable due to the weak dynamic stiffness of toolholder as its length-diameter ratio increases. Using a holder with various cross-sectional diameters along the holding shaft will increase the difficulty to improve its dynamic performance. Therefore, the paper aims to overcome the above challenges to design a novel toolholder by employing passive dynamic control method to suppress chatter and improve MRR. After the introduction, the dynamic model of face milling operation is established in Section 2 to analyse the relationship between milling stability and dynamic parameters of cutter system. Following this, a novel toolholder is designed in Section 3, whose construction and materials are analyzed and optimized. Section 4 identifies the dynamics parameters of the milling cutter with the novel toolholder. Meantime, a series of milling testing are performed to verify the stability of the novel tool and to optimize machining parameters for increasing MRR. Finally, some conclusions are drawn in Section 5.

2. Dynamic modal of face milling operation

A horizontal face milling system including spindle, milling cutter and workpiece is shown in Fig. 1(a), where a four-inserts cutter with a diameter of 80 mm is employed. In Fig.1 (a), the toolholder is composed of six sections with different diameters, varying from 40 mm as the smallest diameter to 70 mm as the largest diameter, whose overhang length-diameter ratio is in the range of [4.5, 7.9]. However, when the length-diameter ratio is over 4, the chatter is easy to occur during milling process [32]. In order to suppress chatter response under the milling system in Fig. 1(a), a dynamic model of face milling operation is built as seen in Fig. 1(b). In the figure, the lumped parameter milling model is described with dampers and springs along three orthogonal degrees of freedom (X, Y and Z). The cutter is regarded as a flexible body, whereas the workpiece is considered as the rigid body. Based on the Newton's laws of motion, the dynamic equation of the face milling system can be expressed as follows [10]:
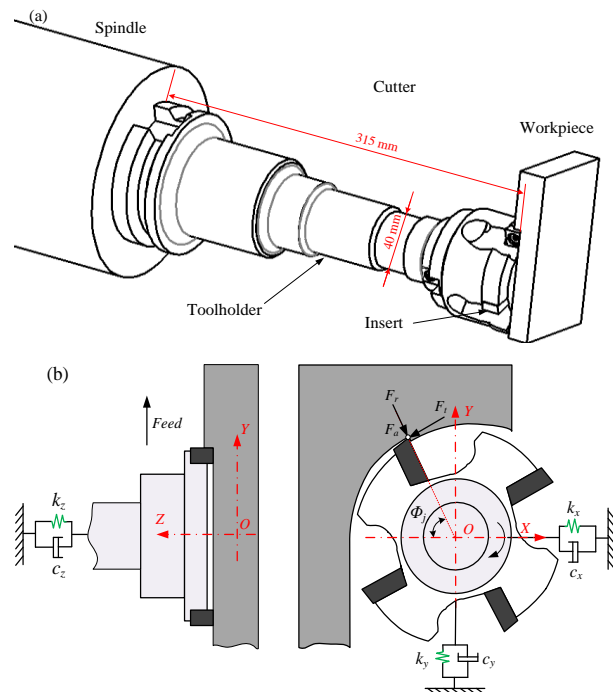
Fig. 1. Schematic diagram of face milling system. (a) Face milling operation with a toolholder with the variable cross-sections and large length-diameter ratio; (b) Dynamic model of face milling operation.

$$\ddot{x}(t) + 2\zeta_x \dot{x}(t) + \omega_{nx}^2 x(t) = \frac{\omega_{nx}^2}{k_x} \sum_{j=1}^{N} F_{x,j}(t)$$

$$\ddot{y}(t) + 2\zeta_y \dot{y}(t) + \omega_{ny}^2 y(t) = \frac{\omega_{ny}^2}{k_y} \sum_{j=1}^{N} F_{y,j}(t) \tag{1}$$

$$\ddot{z}(t) + 2\zeta_z \dot{z}(t) + \omega_{nz}^2 z(t) = \frac{\omega_{nz}^2}{k_z} \sum_{j=1}^{N} F_{z,j}(t)$$

where ζ_γ, k_γ and $\omega_{n\gamma}$ ($\gamma = x, y, z$) refer to the damping ratio, stiffness and natural frequency along three different directions, respectively. $F_{\gamma,j}$ are the cutting forces of tooth j along X, Y and Z directions involved in milling process. N is the number of tooth.

The cutting forces can be represented by the function of the immersion angle of ϕ_j as follows [33]:

$$\begin{Bmatrix} F_{x,j}(t) \\ F_{y,j}(t) \\ F_{z,j}(t) \end{Bmatrix} = \begin{bmatrix} -\sin\kappa\cos(\phi_j) & -\cos(\phi_j) & -\cos\kappa\sin(\phi_j) \\ -\sin\kappa\cos(\phi_j) & \sin(\phi_j) & -\cos\kappa\cos(\phi_j) \\ \cos(\phi_j) & 0 & -\sin\kappa \end{bmatrix} \cdot \begin{Bmatrix} F_{r,j}(t) \\ F_{t,j}(t) \\ F_{a,j}(t) \end{Bmatrix} \tag{2}$$

where κ is the lead angle. $F_{\mu,j}$ ($\mu=r$, t and a) represent the radial, tangential and axial forces acting on the insert j, respectively, which can be written as [34]

$$\begin{Bmatrix} F_{r,j}(t) \\ F_{t,j}(t) \\ F_{a,j}(t) \end{Bmatrix} = \left\{ K_{tc} \cdot \frac{a}{\sin\kappa} \cdot \begin{bmatrix} K_{rc} \\ 1 \\ K_{ac} \end{bmatrix} \cdot h(\phi_j) + \begin{bmatrix} K_{re} \\ K_{te} \\ K_{ae} \end{bmatrix} \cdot S \right\} \cdot g(\phi_j) \tag{3}$$

where $K_{\mu c}$ and $K_{\mu e}$ are the cutting and edge coefficients, respectively. a is the axial depth of cut. S is the length of cutting edge of insert. $h(\varphi_j)$ is the instantaneous dynamic chip thickness, which is denoted as

$$h(\phi_j) = h_s(\phi_j) + h_d(\phi_j) \tag{4}$$

where $h_s(\varphi_j)$ and $h_d(\varphi_j)$ are the static and dynamic chip thickness respectively, which can be described as

$$h_s(\phi_j) = f_z \sin(\phi_j)\sin(\kappa)$$

$$h_d(\phi_j) = \begin{Bmatrix} \sin(\phi_j)\sin(\kappa) & \cos(\phi_j)\sin(\kappa) & -\cos(\kappa) \end{Bmatrix}^T \cdot \begin{Bmatrix} \Delta x \\ \Delta y \\ \Delta z \end{Bmatrix} \tag{5}$$

Here, f_z stands for feed per tooth. Δx, Δy and Δz are the variation of vibration displacement between previous tooth and current tooth along three orthogonal directions.

Then, the cutting forces can be written as the matrix form [10, 35]

$$\begin{Bmatrix} F_x(t) \\ F_y(t) \\ F_z(t) \end{Bmatrix} = a \cdot K_t \cdot [A(t)] \cdot \begin{Bmatrix} \Delta x \\ \Delta y \\ \Delta z \end{Bmatrix} \tag{6}$$

where matrix A refers to the time varying directional dynamic force coefficients, which can be expressed as

$$[A_0] = \frac{1}{2\pi} \int_0^{2\pi} [A(\phi)] d\phi = \frac{N}{4\pi}\alpha \tag{7}$$

Further, the cutting forces can be rewritten in time domain as follows

$$\{F(t)\} = \frac{N}{4\pi} a \cdot K_t \cdot [\alpha] \cdot \{\Delta t\} \tag{8}$$

The dynamic vibration displacement vector Δt is described in frequency domain as follows

$$\{\Delta t(\omega)\} = \{t_j(\omega)\} - \{t_{j-1}(\omega)\}$$
$$= (1 - e^{-i\omega T})[\Phi(i\omega)]\{F(\omega)\} \tag{9}$$

where $\Phi(i\omega)$ is the frequency response function (FRF) of cutter tip, which is defined as.

$$[\Phi(i\omega)] = \begin{bmatrix} \Phi_{xx}(i\omega) & \Phi_{xy}(i\omega) & \Phi_{xz}(i\omega) \\ \Phi_{yx}(i\omega) & \Phi_{yy}(i\omega) & \Phi_{yz}(i\omega) \\ \Phi_{zx}(i\omega) & \Phi_{zy}(i\omega) & \Phi_{zz}(i\omega) \end{bmatrix} \tag{10}$$

Here, $\Phi_{xx}(i\omega)$, $\Phi_{yy}(i\omega)$ and $\Phi_{zz}(i\omega)$ are the direct FRF along three orthogonal degrees of freedom respectively, which can be expressed as considering multiple modes.

$$\Phi_{xx}(i\omega) = \frac{x}{F_x} = \sum_{v=1}^{n} \frac{\omega_{nxv}^2}{k_{xv}(\omega_{nxv}^2 - \omega^2 + i2\zeta_{xv}\omega_{nxv}\omega)}$$

$$\Phi_{yy}(i\omega) = \frac{y}{F_y} = \sum_{v=1}^{n} \frac{\omega_{nyv}^2}{k_{yv}(\omega_{nyv}^2 - \omega^2 + i2\zeta_{yv}\omega_{nyv}\omega)} \tag{11}$$

$$\Phi_{zz}(i\omega) = \frac{z}{F_z} = \sum_{v=1}^{n} \frac{\omega_{nxr}^2}{k_{xv}(\omega_{nyv}^2 - \omega^2 + i2\zeta_{yv}\omega_{nyv}\omega)}$$

Then, Transforming Eq. (8) into the expression by frequency domain, where the frequency domain representation of cutting forces can be performed as

$$\{F(\omega)\} = \frac{N}{4\pi}aK_t(1 - e^{-i\omega T})[\alpha][\Phi(i\omega)]\{F(\omega)\} \tag{12}$$

When the face milling system is under the critical stable state at chatter frequency ω_c, the characteristic equation can be obtained as

$$\det\{[I] + \Lambda[\alpha][\Phi(i\omega_c)]\} = 0 \tag{13}$$

The system eigenvalues are defined as

$$\Lambda = \Lambda_{Re} + \Lambda_{Im} = -\frac{N}{4\pi}aK_t(1 - e^{-i\omega_c T}) \tag{14}$$

The stability limit and the corresponding spindle speeds can be obtained as

$$a_{lim} = -\frac{2\pi}{NK_t}\Lambda_{Re}(1 + \frac{\sin^2(\omega_c T)}{(1 - \cos(\omega_c T))^2})$$

$$\Omega = \frac{60\omega_c}{N(\pi - 2\arctan(\Lambda_{Im}/\Lambda_{Re}) + n \cdot 2\pi)} \quad n=0,1,2,... \tag{15}$$

From the Eq. (15), it is known that the stable limit of milling system depends on the modal parameters of cutter including modal stiffness and damping ratio, when the teeth number and cutting coefficients are constant. Based on the stability prediction model here, the relationship between the limit of axial depth of cut a_{lim} and modal parameters of milling cutter is analysed and is presented in Figs. 2 and 3. As shown in Fig. 2 (a), a_{lim} increases notably with the increase of the first order (FO) modal parameters of cutter. It is worth to note that although the a_{lim} varies in a narrow range with the change of second order (SO) modal parameters in Fig. 2(b), the influence of SO modal parameters on a_{lim} should be considered as well, due to the certain contribution of SO modal parameters on the frequency response function $\Phi(i\omega)$. It is also observed clearly in Fig. 3 that the a_{lim} will increase when FO stiffness or damping ratio increases. Dynamic stiffness can be expressed by the function of modal stiffness and damping ratio [1, 3]. Fig. 4 shows the relationship between a_{lim} and dynamic stiffness, where a_{lim} is increased via

enhancing dynamic stiffness of the cutter. Therefore, the increase of the dynamic stiffness for face milling cutter will expand the milling stability.
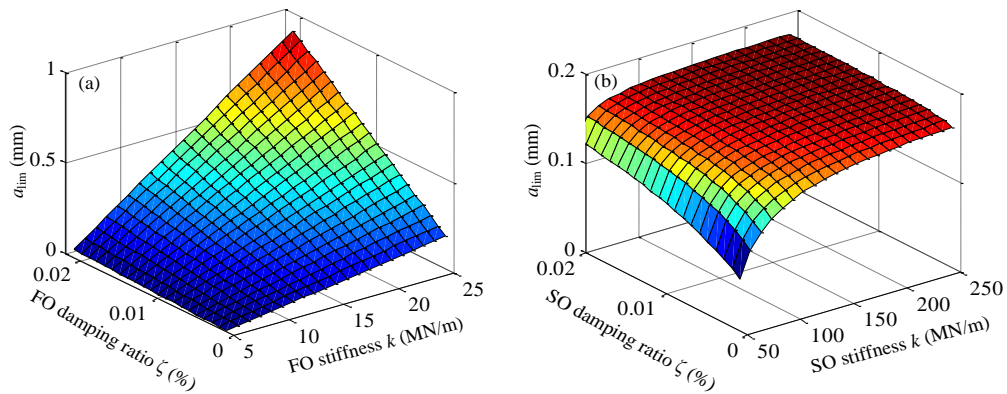
Fig. 2 The relationship between a_{lim} and the first two order modal parameters of toolholder
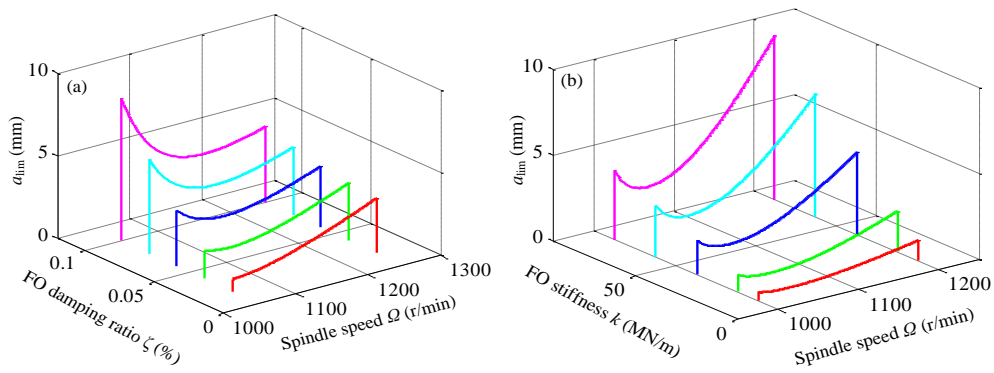
Fig. 3 The relationship between a_{lim} and the first order damping ratio (a) and modal stiffness (b).
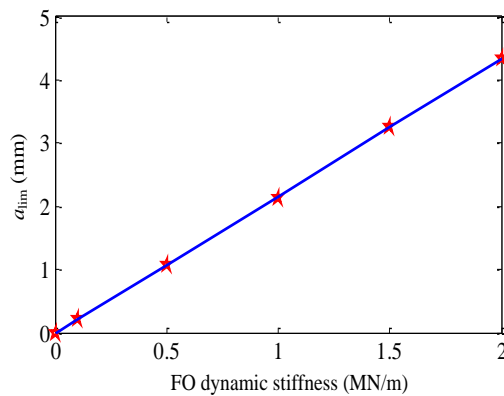
Fig. 4 The relationship between a_{lim} and first order dynamic stiffness.

3. Design and optimization of a novel toolholder

3.1 Structural design of a novel toolholder

With reference to Fig. 1(a), it should be noted that the outer geometrical structure of the conventional toolholder cannot be modified as it is designed for machining the workpiece of special geometrical structure. This increases the difficulty of the new design. However, the theoretical analysis in section 2 provides a useful guideline to the design of a novel toolholder to achieve high stability performance. The main design principles are as follows:

(1) Maintaining the outer geometry shape of the conventional toolholder;

(2) Designing the special stair-step mental strips with high rigidity according to the outer dimension of the toolholder, which are inlaid into the toolholder to improve the whole stiffness.

(3) Filling high damping material into the toolholder hole to increase the damping property of milling cutter.

(4) The weight of the novel toolholder should be less than that of the conventional toolholder considering the characteristic of horizontal machining.

(5) The economic cost for the new toolholder should be taken into account when designing the toolholder.

Following these design principles, a novel toolholder is designed and is shown in Fig. 5.
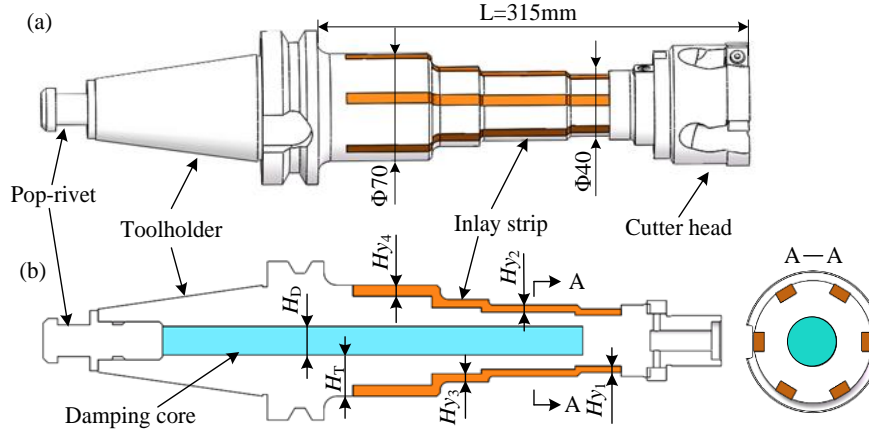
Fig. 5 Geometrical structure design of the novel toolholder. (a) The milling cutter including the novel toolholder and cutter head. (b) The section diagram of the novel toolhoder.

3.2 Damping characteristic analysis

In order to analyse the damping characteristic qualitatively, the toolholder could be simplified as a cantilever beam. The cross-section of a certain segment of the toolholder is illustrated in Fig.6. The damping characteristic of the new toolholder depends on the damping core part, whereas the damping property from both the base body of toolholder and the inlaid strips is ignored attributing to their relative low damping ratio as listed in Table 1.
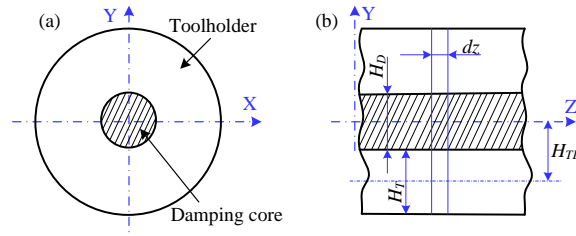
Fig. 6 Cross-sectional parameter relationship between damping core and toolholder.
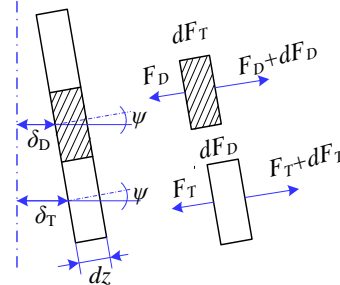
Fig.7 Stress and deformation model of element segment of toolholder.

The strain energy method [3, 36, 37] is employed in the paper used to calculated the loss factor. The subscript symbol χ=T or D denotes the base body of toolholder or damping core, respectively. In terms of deformation model in Fig 7, the relationship between toolholder substrate and damping core can be represented by

$$\delta_T = \delta_D + H_{TD} \cdot \tan\psi \approx \delta_D + H_{TD} \cdot \psi \tag{16}$$

where ψ refers to the angular displacement of element segment caused by bending vibration.

From Fig. 7, the force equilibrium relationship is described as

$$dF_D + F_T + dF_T - F_T = 0 \tag{17}$$

$$(k_T^{'} \frac{d^2(\delta_T)^2}{dz^2} + k_D^{'} \frac{d^2(\delta_D)^2}{dz^2})dz = 0 \tag{18}$$

where

$$k_{\chi}^{'} = \frac{F_{\chi}}{\Gamma_{\chi}} \quad \Gamma_{\chi} = \frac{d\delta_{\chi}(z)}{dz} \tag{19}$$

It is noted that the angle ψ is harmonic, which is defined as

$$\psi(z) = \psi_0 \cos \rho z \tag{20}$$

Thus, Eq. (18) can be rewritten as

$$k_T^{'} \delta_T + k_D^{'} \delta_D = 0 \tag{21}$$

Additionally, the new variable $R_{\chi}^{'}$ is defined as:

$$R_T^{'} = \frac{\delta_T}{\varphi} \quad R_D^{'} = \frac{\delta_D}{\varphi} \tag{22}$$

Substituting Eq. (22) into Eqs. (16) and (21), then $R_{\chi}^{'}$ can be given by

$$R_T^{'} = \frac{k_D^{'} H_{TD}}{k_D^{'} + k_T^{'}} \quad R_D^{'} = \frac{k_T^{'} H_{TD}}{k_D^{'} + k_T^{'}} \tag{23}$$

Thus,

$$\frac{k_D^{'}}{k_T^{'}} = \frac{k_{DR}^{'}(1+i\beta)}{k_{TR}^{'}(1+i\beta_T)} \underset{\beta_T \to 0}{=====} k(1+i\beta) \tag{24}$$

Then, Substitution into Eq. (23) gives Eq. (22).

$$\left| R_T^{'} \right|^2 = \frac{k^2(1+\beta)H_{TD}^2}{(1+k)^2 + (\beta k)^2} \quad \left| R_D^{'} \right|^2 = \frac{H_{TD}^2}{(1+k)^2 + (\beta k)^2} \tag{25}$$

Ignoring the shear deformation energy, the loss factor of the novel toolholder can be expressed by

$$2\zeta = \eta = \frac{\beta(k_{DR}^{'} \left| R_D^{'} \right|^2 + B_D^{'})}{k_{TR}^{'} \left| R_T^{'} \right|^2 + B_T^{'} + k_{DR}^{'} \left| R_D^{'} \right|^2 + B_D^{'}} \tag{26}$$

Substitution Eq. (21) into Eq. (22), loss factor η can be simplified as

$$\frac{\eta}{\beta} = \frac{eh}{(1+eh)} \cdot \frac{3+6h+4h^2+2eh^3+e^2h^4}{1+2e(2h+3h^2+2h^3)+e^2h^4} \tag{27}$$

where β refers to the loss factor of damping material. In addition,

$$e = \frac{E_D}{E_T} \quad h = \frac{H_D}{H_T}$$

From the loss factor formula, the relationship among damping capability of the toolholder, material property and geometrical size are revealed in Figs. 8-9. It can be illustrated in Fig. 8 that the loss factor η of the toolholder increases with the increase of loss factor of damping material β. When h, i.e. the ratio of diameter of damping

core to the thickness of base body, gradually increases, η increases as well in Fig.8 (a), which is validated in Fig. 9 (a). In addition, η becomes large as e increases from the initial value, while it will remain mainly unchanged when e reaches to a larger value, which can be observed from Fig. 9(b). Thus, in order to improve the damping performance of the toolholder, it is essential to choose the material with high β and suitable E_D made the core filler. The diameter H_D of the damping core should be designed suitably to keep high loss factor of thetoolholder while keeping its high rigidity.
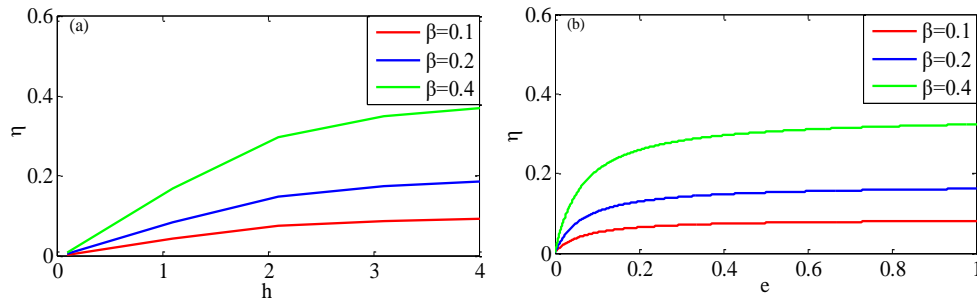
Fig. 8 Loss factor of toolholder in terms of h, e and β.
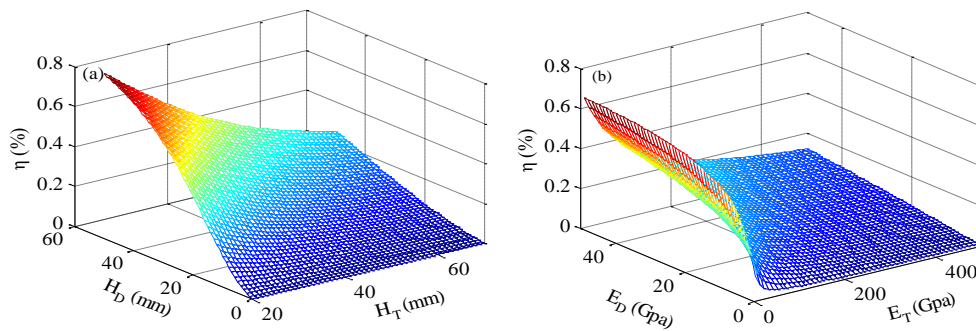
Fig. 9 The relationship between loss factor and geometrical parameters and elastic modulus of parts.

3.3 Stiffness characteristic analysis

The stiffness characteristic of the cantilever beam can be expressed as [1]

$$k = \frac{3(\text{EI})_{eq}}{L^3} \tag{28}$$

where $(\text{EI})_{eq}$ refers to the equivalent bending stiffness. E is the elasticity modulus of material. I is the inertia moment. L is the length of cantilever beam.
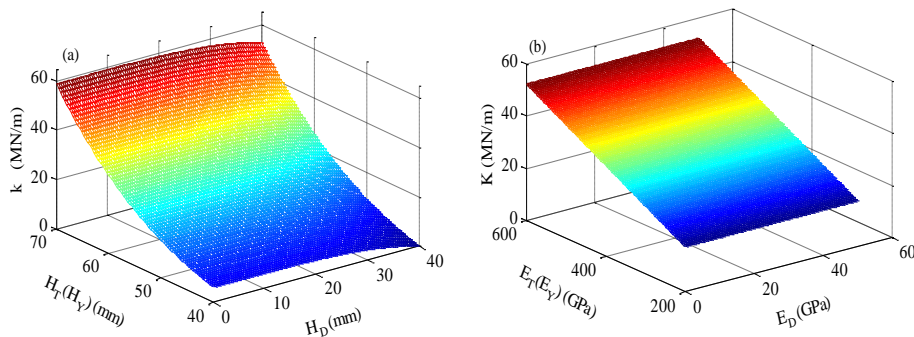
Fig.10 The relationship between the stiffness characteristic and geometrical parameters (a) and elastic modulus (b) of parts.

According to the Eq. (28), the stiffness of cantilever beam k is determined by the cross-section shape and elasticity modulus. Then, the relationship curve between stiffness characteristic of the toolholder and the physical size and elasticity modulus of the different parts is ploted in Fig. 10. As shown here, the stiffness value of

toolholder k increases as the diameter of damping core H_D decreases or the thickness of base body (inlaid strips) H_T (H_Y). The increasing $E_T(E_Y)$ would improve the stiffness value of toolholder in Fig. 10(b), while the elasticity modulus of damping material E_D has a little effect on the stiffness characteristic due to the small value. Therefore, the size of various parts for toolholder should be determined suitably to maximize the stiffness for improving the rigidity performance and guaranteeing the damping property of toolholder.

3.4 Structural optimization and material selection of the novel toolholder

From the above qualitative analysis for the dynamic characteristics, it is clearly obtained that the geometrical parameters and material property of the damping core and inlaid strips have a directly effect on the damping and stiffness features for toolholder. The damping ratio of toolholder will rise with the increase of the diameter and elastic modulus of damping core, while the damping ratio will remain constant when the elastic modulus reaches some certain value. Similarly, the stiffness of toolholder will enlarge as the section diameter size and elastic modulus of main body or the inlaid strip. However, the increase of diameter for damping core invariably leads to a decrease of stiffness of toolholder. Thus, it is crucial to optimize the size and select the corresponding material for the damping core and inlaid strips of the novel toolholder.

For the toolholder, the material of base body is 35CrMo steel. Due to the high modulus, YG6 carbide in Table 1 is used to make the inlaid strips. The high damping materials, such as foamed aluminium, epoxy rubber, polymethyl methacrylate and polyurethane rubber, are selected as the candidate materials of damping core, where the properties of these materials are listed in Table 1. Then, the schemes for the novel toolholder with different material combinations are made as shown in Table 2.

Table. 1 Material properties of toolholder

Material	Density (g/cm^3)	Elastic modulus (GPa)	Poisson's ratio	Material loss factor (%)
35CrMo steel	7.87	213	0.29	0.1
YG6 carbide	14.5	600	0.21	0.1
Foamed aluminium (FA)	0.65	12	0.33	12
Epoxy rubber (ER)	1.15	6.9	0.4	10
Polymethyl methacrylate (PM)	0.51	10	0.3	20
Polyurethane rubber (PR)	1.11	30	0.3	47

Table. 2 Comparsion of the toolholder with different material combination

Part	Conventional toolholder	Novel toolholder			
Case	1	2	3	4	5
Base body			35CrMo		
Inlaid strip	35CrMo		YG6		
Damping core		FA	ER	PM	PR

As shown in Fig. 5, several mental strips are inlaid into the base body of toolholder, where the number of strips will affect the overall stiffness of toolholder. The relationship among stiffness characteristic, strip number and economic cost is analysed in Fig. 11. The stiffness will increase as the number of strips increases, while the corresponding cost will also increase significantly. In order to control cost and guarantee high stiffness performance, the six strips are selected to inlay into the novel toolholder. In addition, the embedded strip consists of four segments, where H_{y1}, H_{y2}, H_{y3} and H_{y4} stand for the corresponding thickness values, respectively. For the convenience of structural optimization, the thickness values of four segments for the inlaid strips are assumed to

be proportional to the diameter size of the corresponding cross section in the toolholder. Thus, the thickness H_{y1} is set as the optimization parameter for stiffness characteristic.
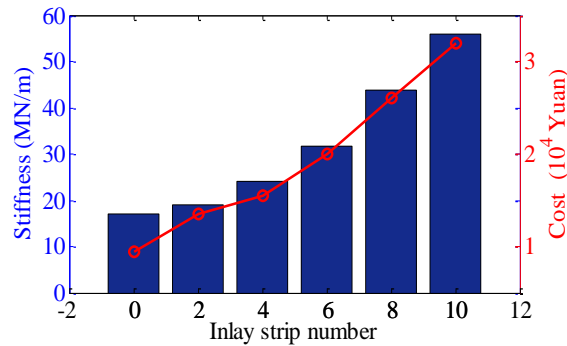
Fig. 11 The relationship among the inlay strip number, stiffness and cost.

To optimize the structural parameters of the combination schemes for the novel toolholder in Table 2, the finite element method is employed. In the optimization process, three main steps are required, including: (1) set H_T and H_{y1} as design variables and the minimum frequency response amplitude as the objective function, (2) perform the Harmonic Response and Goal Drive Optimization analysis, and (3) obtain the optimal parameter values and the corresponding response amplitudes as shown in Table 3. The dynamic stiffness can be obtained from the response amplitude curves, which are listed in Table 3 as well. Then, the analysis results are exhibited intuitively in Fig. 12. It can be presented clearly that the novel toolholder with 35CrMo-YG6-PR combination has the highest dynamic stiffness and the lowest response amplitude, which shows the best dynamic performance. Finally, the novel toolholder is made by using the design parameters in Case 5. The weight of new cutter is 9.2 kg is less than that of the conventional cutter with 9.4 kg. The novel cutter meets the design and application requirement of the dynamic balance after detecting.

Table. 3 Parameter design and the dynamic responses.

Case	Design dimension (mm)		Dynamic stiffness (MN/m)	Response amplitude (um)
	H_D	H_{Y1}		
1	-	-	0.21	5.11
2	18.83	4.03	0.68	1.53
3	18.91	3.96	0.66	1.58
4	18.61	4.12	0.71	1.47
5	18.14	4.20	0.75	1.35
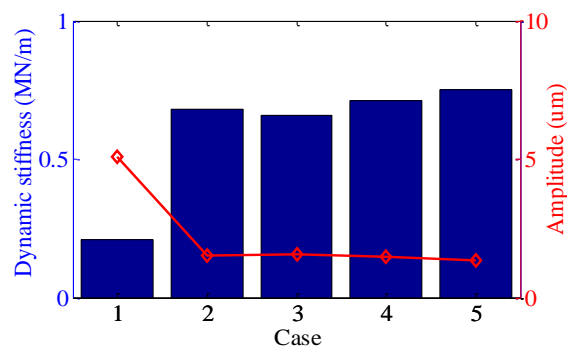
Fig. 12 Dynamic stiffness and response amplitude of the corresponding toolholder.

4. Experimental testing and analysis

4.1 Tool point dynamics of milling cutter with the novel toolholder

The dynamic behaviours that occur at the tip of face milling cutter should be predicted accurately so as to better understand the milling stability. Typically, the transfer function for a machining system is identified using

structure dynamics tests [35, 38, 39]. An impact hammer (CL-YD-303) is employed to excite the tool tip and the data acquisition system (Pulse 3560C) is applied to collect the impulse load and tool response signals in Fig. 13 (a), where the conventional and novel cutters are mounted on the spindle in a horizontal CNC machining center (SPN50R) in turn in Fig. 13(b).
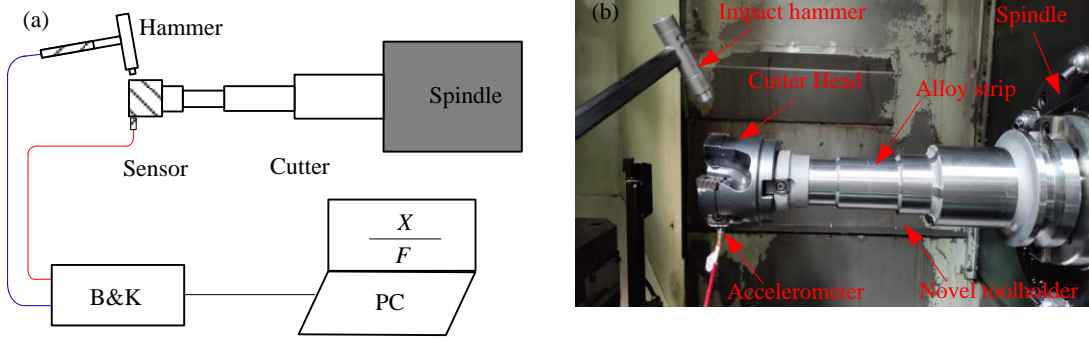
Fig. 13. Modal testing. (a) Schematic diagram of modal experiment; (b) experiment setup.

From Eq. (11), the direct frequency response function $\Phi_{\gamma\gamma}$ (γ=x, y and z) can be obtained by collecting the response at cutter tip and the impulse load from the hammer along the identical coordinate direction, where the cross FRFs are neglected. The Eq. (11) can be rewritten by as follows:

$$\mathrm{Re}(\Phi_{\gamma\gamma}) = \sum_{v=1}^{n} \frac{1}{k_{\gamma v}} \frac{1-r_v^2}{(1-r_v^2)^2 + (2\zeta_{\gamma v}r_v)^2}$$

$$\mathrm{Im}(\Phi_{\gamma\gamma}) = \sum_{v=1}^{n} \frac{1}{k_{\gamma v}} \frac{-2\zeta_{\gamma r}r_v}{(1-r_v^2)^2 + (2\zeta_{\gamma v}r_v)^2}$$

(29)

where $r_v=\omega/\omega_n$ stands for the frequency ratio of v-th order mode.

After dynamic tests, the measured FRFs at the tip of two cutters along X and Y directions are shown in Figs. 14 and 15, in which the corresponding fitting curves are obtained by modal fitting method [35].
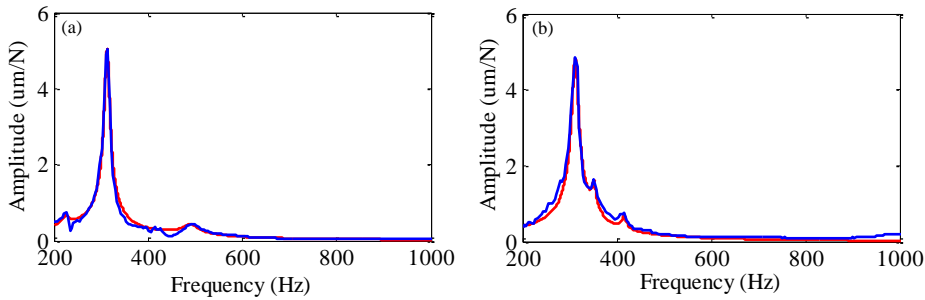
Fig. 14 Measured (blue line) and fitting (red line) FRFs at tip of the conventional cutter
along X (a) and Y (b) directions respectively.
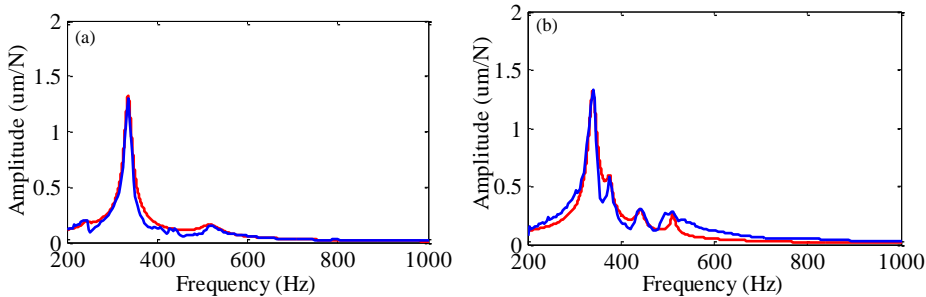
Fig. 15 Measured (blue line) and fitting (red line) FRFs at tip of the novel cutter
along X (a) and Y (b) directions respectively.

Table 4. Modal parameters of milling cutter with the conventional toolholder

		Frequency ω_n (Hz)	Damping ratio ζ (%)	Stiffness k (MN/m)
X-Modes	1	314	1.27	7.82
	2	492	3.26	49.59
Y-Modes	1	312	1.28	8.07
	2	352	2.01	55.12
	3	416	0.752	173.2
Z-Modes	1	284	1.41	275.06

Table 5. Modal parameters of milling cutter with the novel toolholder

		Frequency ω_n (Hz)	Damping ratio ζ (%)	Stiffness k (MN/m)
X-Modes	1	336	2.38	16.12
	2	520	2.29	106.67
Y-Modes	1	340	2.35	16.08
	2	376	1.42	114.83
	3	442	0.81	319.85
Z-Modes	1	284	2.11	226.24

According to the peak picking method, the modal parameters of the two cutters are obtained from the fitting curves as listed in Tables 4 and 5. The first order modes for the two cutters along X and Y directions are the main mode, namely target mode, while the second modes should be considered when calculating the SLD due to the certain effect on the response. The FRF along Z direction is neglected owing to the larger orders of magnitude of modal parameters than those in X and Y directions. Comparing with the conventional toolholder, both the main damping ratio and stiffness of the novel toolholder show a clear increase. The main dynamic stiffness of the conventional cutter in X and Y directions are 0.198 MN/m and 0.207 MN/m respectively, while the corresponding values of the novel toolholder are 0.767 MN/m and 0.756 MN/m, which shows that the growth rate of dynamic stiffness is about 3.75 times and thus effectively improve the milling stability performance.

4.2 Face milling stability analysis

After analysis of the dynamic characteristics of the two cutters, the stability lobe diagram (SLD) can be constructed by FRFs considering multi-order modes as seen in Eq. 29. The obtained SLD for the conventional and novel cutters are demonstrated in Fig. 16. From the figure, it can be found that the axial critical depth of cut with the novel cuter is about 1.65 mm, while that is 0.44 mm using the conventional cutter.
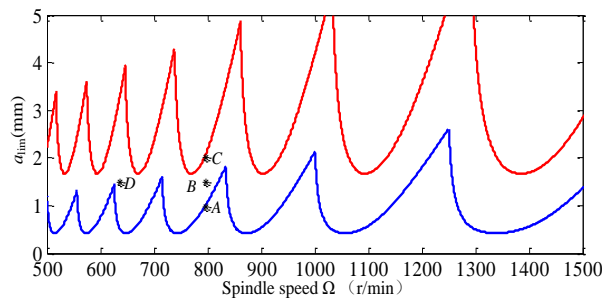
Fig. 16 Stability lobe diagrams of face milling operations with the conventional (blue line) and designed (red line) cutters.

In order to verify the milling stability for the novel cutter, the milling experiments were carried out in the horizontal CNC machining center (SPN50R). A type of designed workpieces with the material of gray iron were utilized to perform the milling testing with the variation of a_{lim}. To detect the milling stability status, the milling forces acted on the workpiece were collected by the Dynamometer during the experiment process, in which the testing principle was described in Fig. 17(1). The milling experiment setup was shown in Fig. 17 (b).
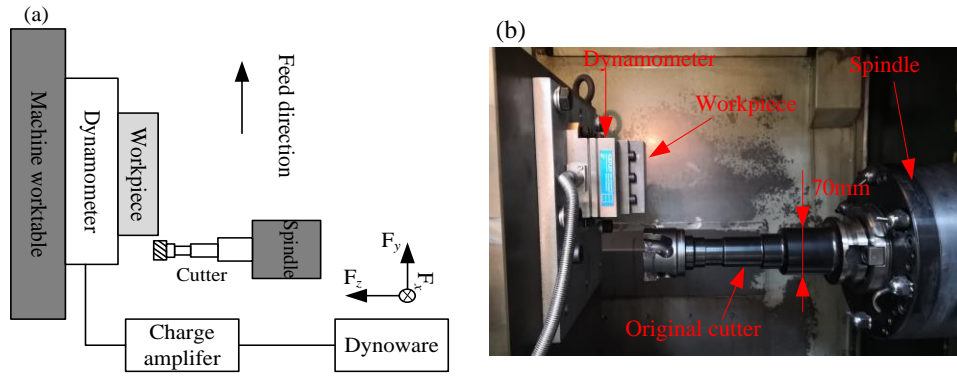
Fig. 17 Milling experiment setup. (a) Schematic diagram; (b) Photograph of milling testing

According to the SLD, three milling conditions were selected to compare the differences of milling stability with the two cutters. The axial depth of cut a varied from 1mm (Case A), 1.5 mm (Case B) to 2 mm (Case C), when the spindle speed Ω with 796 r/min and feed rate f with 31 mm/min were constant, which are consistent with the actual machining parameters in the workshops. The corresponding measured milling forces along X and Y directions are shown in Figs.18-20. In these figures, the rotational frequency ω_r is equal to 13.27 Hz, where the tooth passing frequency ω_f is 53.1 Hz.

In Fig. 18, the axial depth of cut a is 1 mm. It can be seen that the multiplication frequencies (ω_r, $2\omega_r$, $3\omega_r$, …) are the dominant responses, which show the milling states are stable when the conventional and novel cutters are used respectively. When a increases to 1.5mm, i.e. Case B condition, the combination frequencies, i.e. 314.3Hz, 367.5 Hz, 407.2 Hz and 420.4 Hz, can be observed with the conventional cutter in Figs. 19 (a)-(b), while there only appear the multiplication frequencies using the novel cutter in Figs. 19(c)-(d). According to the above modal analysis in section 4.1, the first order natural frequency of the conventional cutter ω_{no} is 314 Hz or 312 Hz. The first order natural frequencies of the conventional cutter along X and Y directions can be regarded as the same value owing to the small difference between the two natural frequencies which may be resulted from the asymmetry structure of machine tool. Thus, these combination frequencies are close to 314 Hz (ω_{no}), 367.1 Hz ($\omega_{no} + \omega_f$), 407 Hz ($\omega_{no} + 7\omega_r$), 420.4 Hz ($\omega_{no} + 8\omega_r$) [18, 40], which mean that the system is under unstable state. In other words, the milling chatter would occur by the conventional cutter under a =1.5mm. By contrast, the evident amplitudes of milling force are not excited under these combination frequencies when the novel cutter is used, which shows it is stable state. The axial depth of cut increases further to 2.0mm. Similarly, the peak values of milling forces with the conventional cutter always appear in the multiple frequency components such as 312.4 Hz, 365.6 Hz, 624.9 Hz and 678 Hz, where these frequencies are around 312 Hz (ω_{no}), 365.1 Hz ($\omega_{no}+ \omega_f$), 624 Hz ($2\omega_{no}$), 677.1 Hz ($2\omega_{no}+ \omega_f$). Comparing to the resulting milling forces from Case B in Figs. 19(a)-(b) and Case C in Figs. 20 (a)-(b), it can be clearly found that the chatter using the conventional cutter under $a = 2$ mm is more severe than that under $a = 1.5$ mm. Apparently, the milling system with the novel cutter becomes slightly unstable when a reaches to 2 mm, where the complex frequency components reveals the occurrence of the chatter in Figs. 20 (c) and (d) [41]. According to the above analysis, under the same case conditions, the stability with the novel toolholder is improved significantly compared to these with the conventional toolholder, which is in agreement with the results from the SLD in Fig. 16.
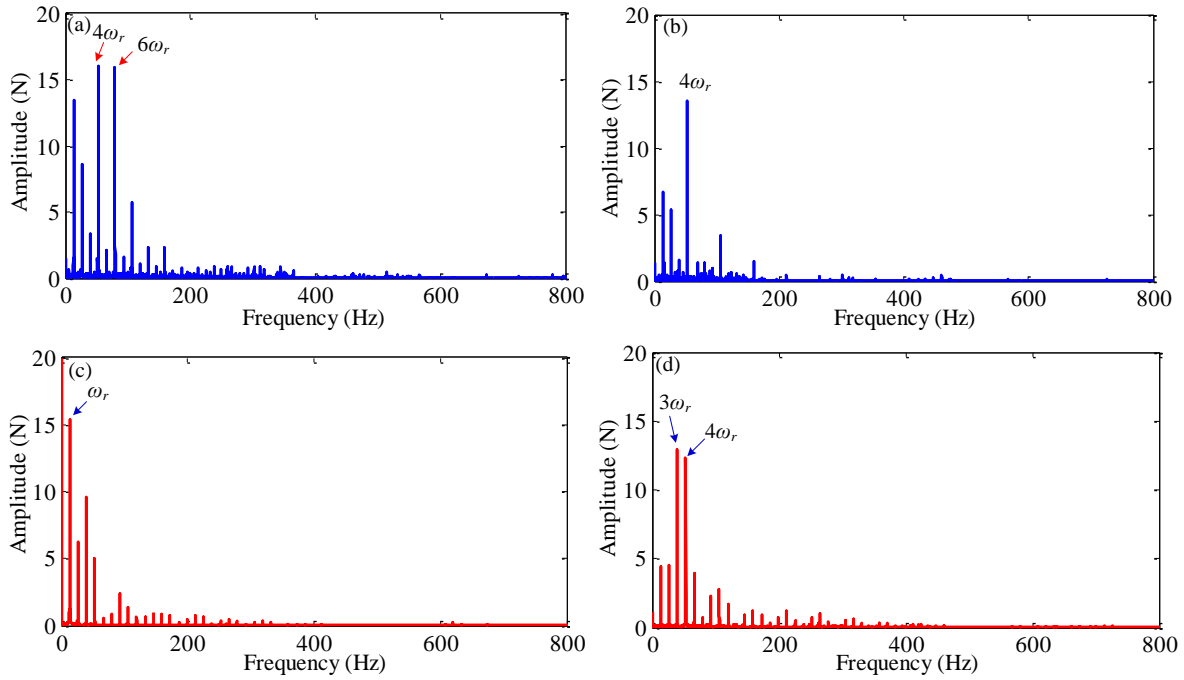
Fig. 18 FFT milling forces along X and Y directions using the conventional (a, b) and novel (c, d) cutters in Case A
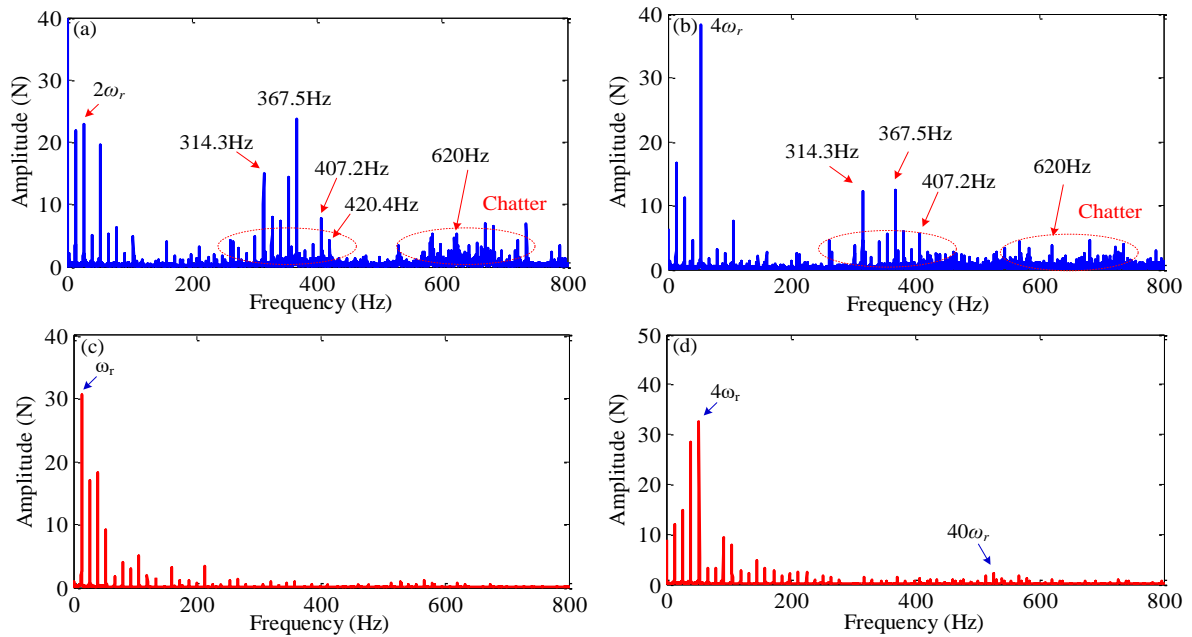
Fig. 19 FFT milling forces along X and Y directions using the conventional (a, b) and novel (c, d) cutters in Case B
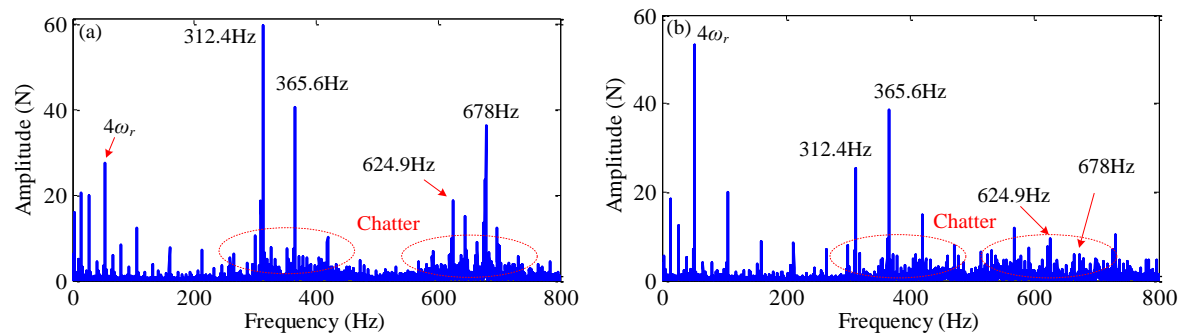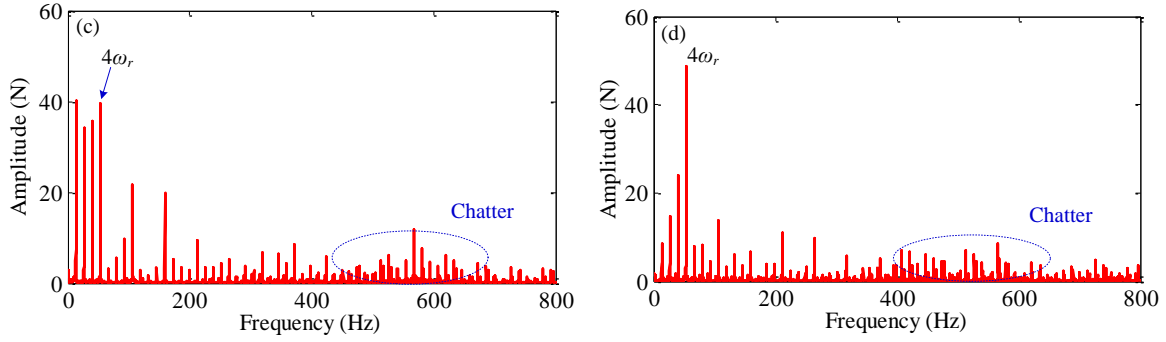
Fig. 20 FFT milling forces along X and Y directions using the conventional (a, b) and novel (c, d) cutters in Case C

In addition, when using the novel toolholder in Case C, the MRR can be increased by 1.33 times comparing to the Case B using the conventional toolholder, where the corresponding chatter using the novel toolholder is far less than that with the conventional cutter.

The material removing rate (MRR) can be expressed by the following equation [42]:

$$MRR = V \times f \times a \tag{29}$$

where $V = \pi D \Omega$ is the cutting velocity in m/min, and D is the dimeter of cutter head.

According to the Eq. (29), in order to improve the MRR, it is selected empirically to decrease spindle speed and increase feed rate when the axial depth of cut keep constant, which is consistent with the actual operation from the workshop experience. Thus, the milling parameters in Case D' including spindle speed Ω with 636r/min, feed rate f with 87 mm/min and axial depth of cut a with 1.5mm, are chosen to analyse the machining stability when using the two cutters, while the feed rate f is 31 mm/min in Case D of SLD in Fig. 16. The resulting milling forces in Case D' condition are shown in Figs. 21-22, respectively. When Ω is 636r/min, the rotational frequency ω_r is equal to 10.6 Hz. Comparing Fig. 21 (a)-(b) with Fig.19 (a)-(b), the amplitudes of milling force at chatter frequency in Fig. 21 are obvious larger than those in Fig. 19, where 324.6 Hz ($\omega_{no} + \omega_r$), 649 Hz ($2\omega_{no} + 2\omega_r$) and 660.2 Hz ($2\omega_{no} + 3\omega_r$) appear as the new chatter frequencies. This is due to the fact that the machining parameters in Case D' make the conventional cutter system unstable, which would be similar to that in Case D of SLD in Fig.16. However, there generates the chatter phenomenon as shown in Fig. 22 when the novel toolholder is used in Cased D', which seems to deny the result of Case D in SLD with the new toolholder. According to the SLD, the chatter would not occur when using the novel toolholder in Case D. It is because the feed rate f is increased from 31 mm/min in Case D to 87 mm/min in Case D'. Even though the process is not stable in Case D' when using the novel toolholder, the amplitude of vibration responses in Fig. 22 are less weak comparing to those with the conventional toolholder in Fig. 19 (c)-(d). Therefore, the novel toolholder can improve the MRR by 2.81 times in Case D' comparing to that in Case B with the conventional toolholder during roughing milling operation.
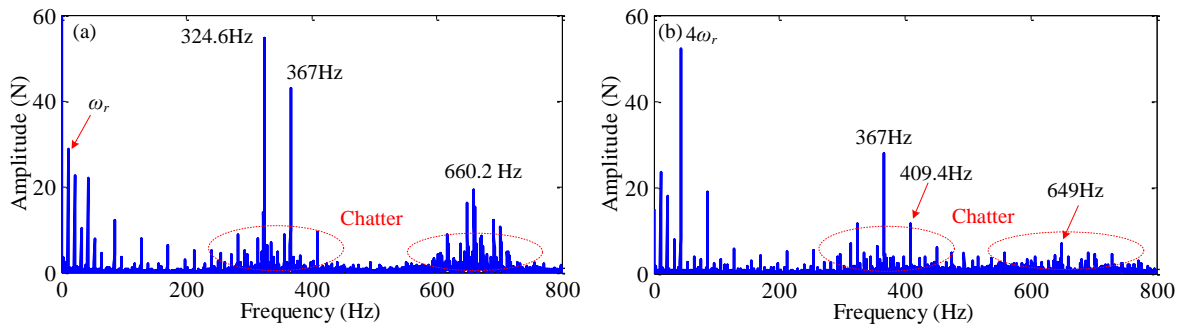
Fig. 21 FFT milling forces along X and Y directions using the conventional cutter in Case D'
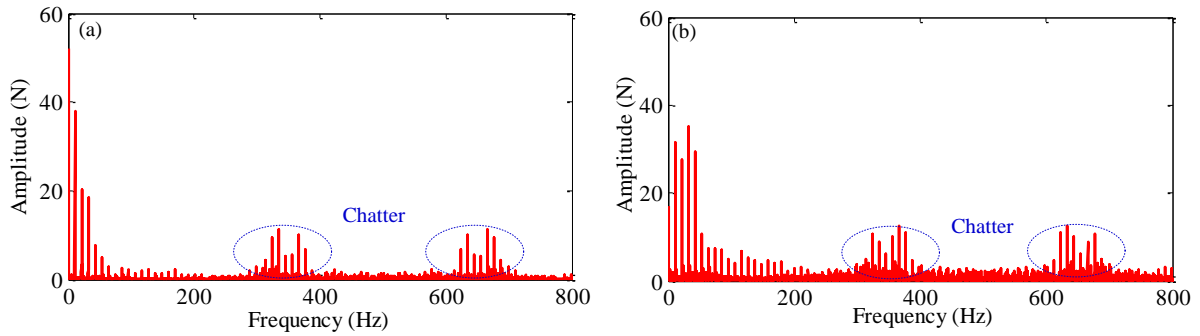
Fig. 22 FFT milling forces along X and Y directions using the novel cutter in Case D'

4.3 Application case: flat face milling operation of motor shell

   To analyse and verify further the milling performance of the two cutters under the above machining conditions, the actual milling operations were performed in the workshops as shown in Fig. 23 (a). The motor shell applied to the engineering machinery was selected as the workpiece, which is made with cast iron. The shell had the characteristic of complex internal cavities as shown in Fig. 23 (b), where the internal bottom surface was required to be machined by face milling operation. However, the vibration signals from the cutter could not be measured directly, since the cutter was inside the shell cavity during milling process. Thus, the dynamic responses of the shell along *X* and *Y* directions were acquired by using the puny accelerometer sensors and then were analysed by B&K data acquisition system as shown in Fig. 23(c). The sensors were mounted on the external plane of shell and was in the same vertical plane with the machined surface, which ensured the accuracy of the collected vibration signals.
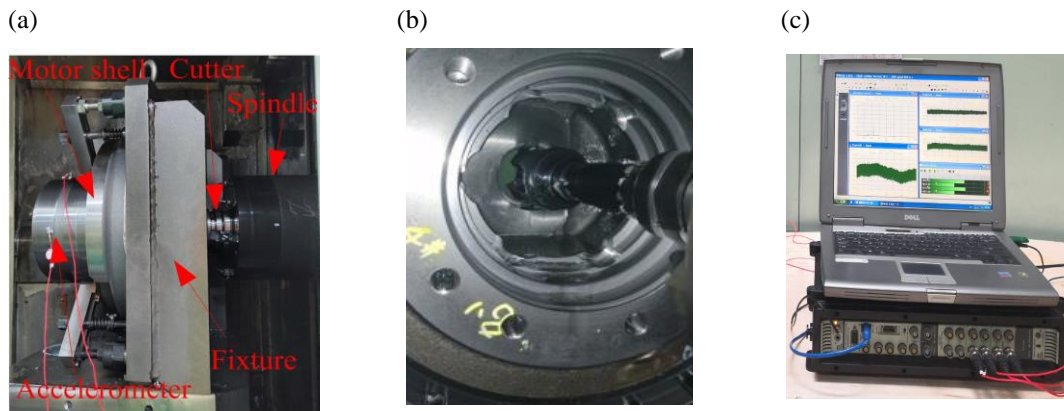
Fig. 23 Experiment setup. (a) Photograph of milling motor shell; (b) Internal view of relative position between cutter and the motor shell; (c) Acceleration signal acquisition system

   The experimental results are shown in Figs. 24-26. It can be found in these figures that the chatter appears at similar frequency values seen from the milling forces analysis. When using the conventional cutter, the vibration responses in Case D' condition in Fig. 25 are more drastic than those in Case B condition in Fig. 24, which obtain the same conclusion from the corresponding milling forces analysis. However, when using the novel cutter in Case D' condition, there only appear smaller vibration responses in Fig. 26 than those with the conventional cutter in Fig. 24. This means that the MRR is increased by 2.81 times when the novel cutter is used under the Case D' condition, while the resulting vibration responses are still smaller. The novel toolholder have now been utilised in the KSD company successfully, which decrease the machining cost markedly.
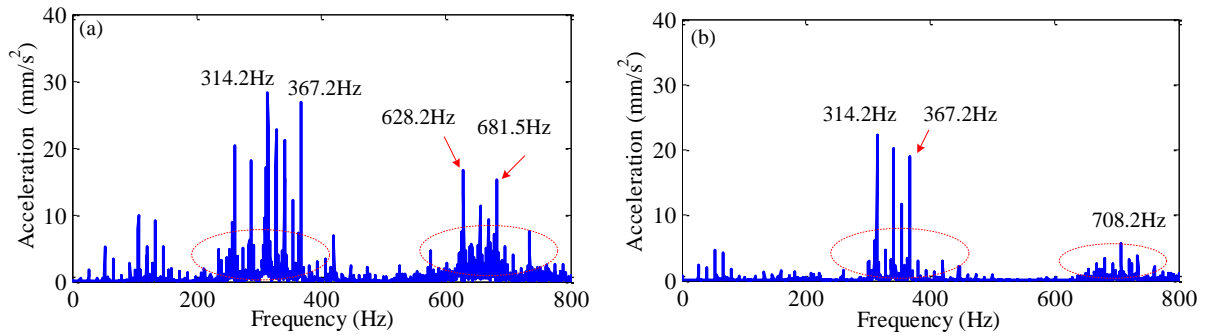
Fig. 24 Acceleration responses along *X* and *Y* directions using the conventional toolholder in Case B.
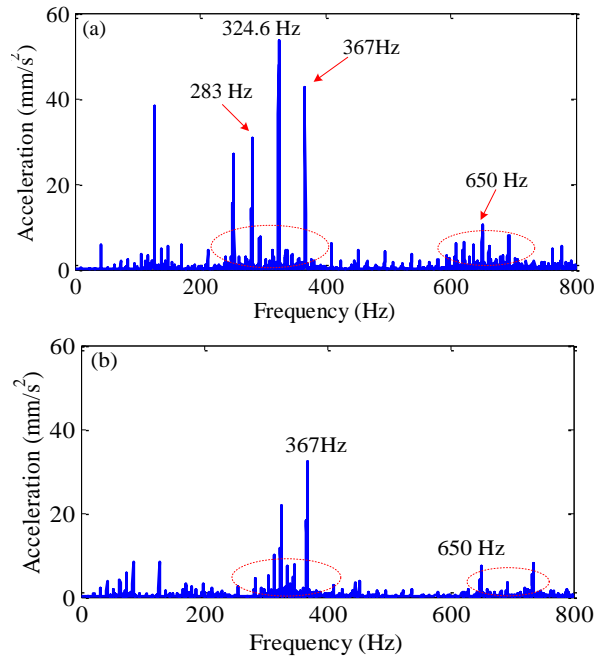
Fig. 25 Acceleration responses along X and Y directions using the conventional cutter under Case D'.
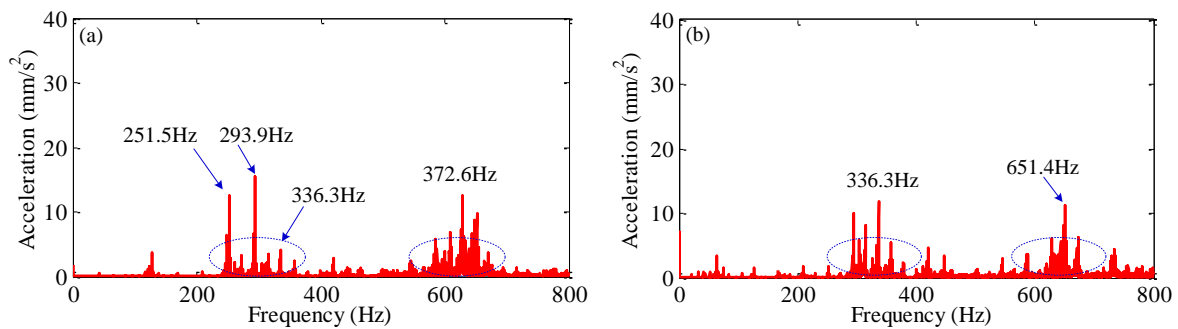
Fig. 26 Acceleration responses along X and Y directions using the novel toolholder in Case D'.

5. Conclusions

To mitigate chatter and enhance MRR in face milling process, this paper developed a novel toolholder to improve the damping and stiffness characteristics of the cutting system, even the toolholder has a large ratio of length to diameter and variable cross-sections to suit specific machining tasks. The key conclusions are reached from this study as following:

(1) According to the dynamic model of face milling operation, the limit of axial depth of cut depends on the modal characteristics of cutter, whose the first and second orders modal parameters should be considered.

(2) A novel toolholder is developed according to the designed principles, where the inlaid strips and damping core are used to improve its dynamic performance. The damping effect is increased with the increase of the diameter of the damping core, while the decrease of the corresponding thickness of the base body of the toolholder would lead to the reduction of stiffness of the toolholder. Based on this finding, the structure parameters and materials for the toolholder are optimized and determined by the finite element method. The optimal combbination for the novel toolholder is to use 35CrMo-YG6-PR with H_D of 18.14mm and H_{y1} of 4.2 mm.

(3) Tool point dynamics tests showed that the first order average dynamic stiffness were increased from 0.203 MN/m to 0.762 MN/m when using the novel toolholder.

(4) The face milling stability of the novel toolholder was verified by milling experiments. When using the design toolholder, the limit of axial depth of cut a_{lim} was increased from 0.44 mm to 1.65 mm.

(5) When using the novel toolholder in Case D' condition with feed rate of 87 mm/min, the chatter is far less than that using the conventional toolholder in Case B condition with feed rate of 31 mm/min. Although the chatter occurs slightly, the MRR was increased by 2.81 times, which can be used in the roughness milling process. The novel toolholder has been applying at the workshop in KSD company, which verifies virtually the analysis and experimental results.

Acknowledge

References

[1] D.G. Lee, H.Y. Hwang, J.K. Kim, Design and manufacture of a carbon fiber epoxy rotating boring bar, Compos. Struct. 60(2003), 115-124.

[2] M. Wan, X.B. Dang, W.H. Zhang, Y. Yang, Optimization and improvement of stable processing condition by attaching additional masses for milling of thin-walled workpiece, Mech. Syst. Signal Process. 103 (2018):196-215.

[3] Q. H. Song, J.H. Shi, Z.Q. Liu, Y. Wan, F. Xia, Boring bar with constrained layer damper for improving process stability, Int. J. Adv. Manuf. Technol. 83 (2016): 1951-1966.

[4] J. Gao, Q.H. Song, Z.Q. Liu, Chatter detection and stability region acquisition in thin-walled workpiece milling based on CMWT, Int. J Adv. Manuf. Technol. 98 (2018): 699-713

[5] G. Quintana, J. Ciurana, Chatter in machining processes: a review, Int. J. Mach. Tools Manuf. 51 (2011): 363-376.

[6] J. Munoa, X. Beudaert, Z. Dombovari, Y. Altintas, E. Budak, C. Brecher, G. Stepan, Chatter suppression techniques in metal cutting, CIRP Ann. - Manuf. Technol. 65(2016):785-808

[7] C.X. Yue, H.N. Gao, X.L. Liu, S.Y. Liang, L.H. Wang, A review of chatter vibration research in milling, Chin. J. Aeronaut. 32(2019):215-242.

[8] H.E. Merrit, Theory of self-excited machine-tool chatter-contribution to machine tool chatter research-1, ASME J. Eng. Ind. (1965) 447–454

[9] Y. Altintas, E. Budak, Analytical prediction of stability lobes in milling, CIRP Ann. Manuf. Technol. 44(1995):357-362.

[10] Y. Altintas, G. Stepan, D. Merdol, Z. Dombovari, Chatter stability of milling in frequency and discrete time domain, CIRP J. Manuf. Sci. Technol. 1(2008): 35-44.

[11] T. Insperger, G. Stépán, Updated semi-discretization method for periodic delay-differential equations with discrete delay, Int. J. Numer. Meth. Eng. 61 (2004) 117-141.

[12] X.F. Dong, W.M. Zhang, S. Deng, The reconstruction of a semi-discretization method for milling stability prediction based on Shannon standard orthogonal basis, Int. J Adv. Manuf. Technol. 85(2016): 1501-1511.

[13] Y. Ding, L.M. Zhu, X.J. Zhang, H. Ding, A full-discretization method for prediction of milling stability. Int. J. Mach. Tools Manuf. 50(2010):502-509.

[14] T. Insperger, Full-discretization and semi-discretization for milling stability prediction: some comments, Int. J. Mach. Tools Manuf. 50(2010):658-662.

[15] M. Lamraoui, M. Barakat, M. Thomas, M. E. Badaoui, Chatter detection in milling machines by neural network classification and feature selection, J. Vib. Control, 21(2015):1251-1266.

[16] H.R. Cao, Y.T. Yue, X.F. Chen, X.W. Zhang, Chatter detection based on synchrosqueezing transform and statistical indicators in milling process, Int. J. Adv. Manuf. Technol. 95(2018): 961-972.

[17] A. Devillez, D. Dudzinski, Tool vibration detection with eddy current sensors in machining process and computation of stability lobes using fuzzy classifiers, Mech. Sys. Signal Process. 21 (2007): 441-56.

[18] M. Wan, T.Q. Gao, J. Feng, W.H. Zhang, On improving chatter stability of thin-wall milling by prestressing, J. Mater. Process. Technol. 264 (2019): 32-44.

[19] C. Peng, L. Wang, T.W. Liao, A new method for the prediction of chatter stability lobes based on dynamic cutting force simulation model and support vector machine, J. Sound Vib. 354 (2015):118-131.

[20] E. Gourc, S. Seguy, L. Arnaud, Chatter milling modeling of active magnetic bearing spindle in high-speed domain, Int. J. Mach. Tools Manuf. 51 (2011): 928-36.

[21] D.H. Li, H.R. Cao, X.W. Zhang, X.F. Chen, R.Q. Yan, Model predictive control based active chatter control in milling process, Mech. Sys. Signal Process. 128 (2019): 266-81.

[22] C. Brecher, D. Manoharan, U. Ladra, H.G. Kopken, Chatter suppression with an active workpiece holder, Prod. Eng. 4 (2010): 239-45.

[23] J. Munoa, X. Beudaert, K. Erkorkmaz, A. Iglesias, A. Barrios, M. Zatarain, Active suppression of structural chatter vibrations using machine drives and accelerometers, CIRP Ann. 64 (2015): 385-88.

[24] R.S. Hahn, Design of lanchester damper for elimination of metal cutting chatter, J. Eng. Industry 73(1951):331–335

[25] K. Kiran, D. Axinte, A. Becker, A Solution for Minimising Vibrations in Milling of Thin Walled Casings by Applying Dampers to Workpiece Surface, CIRP Ann. Manuf Technol. 62 (2013): 415-418

[26] H. Yuan, M. Wan, Y. Yang, Design of a tunable mass damper for mitigating vibrations in milling of cylindrical parts, Chin. J. Aeronaut. 32 (2019): 748-58.

[27] W.S. Ma, Y.Q. Yang, J.J. Yu, General routine of suppressing single vibration mode by multi-dof tuned mass damper: application of three-dof, Mech. Syst. Signal Process 121(2019): 77-96.

[28] Y.Q. Yang, Y.F. Wang, Q. Liu, Design of a milling cutter with large length-diameter ratio based on embedded passive damper, J. Vib. Control 25 (2019): 506-16.

[29] R. Madoliat, S. Hayati, A. Ghasemi Ghalebahman, Investigation of chatter suppression in slender endmill via a frictional damper, Sci. Iran. 18 (2011): 1069-77.

[30] Y. Liu, Z.Q. Liu, Q.H. Song, B. Wang, Development of constrained layer damping toolholder to improve chatter stability in end milling, Int. J. Mech. Sci. 117(2016): 299-308.

[31] E. Rivin, H. Kang, Enhancement of dynamic stability of cantilever tooling structures, Int. J. Mach. Tools Manuf. 32 (1992):539-561.

[32] H.M. Zhou, C.Y. Wang, Z.Y. Zhao, Dynamic characteristics of conjunction of lengthened shrink-fit holder and cutting tool in high-speed milling, J. Mater. Process. Techno. 207(2008): 154-62.

[33] Y. Altintas, Analytical prediction of three dimensional chatter stability in milling, JSME Int. J. Series C 44(2001): 717-23.

[34] A. Iglesias, J. Munoa, J. Ciurana, Optimisation of face milling operations with structural chatter using a stability model based process planning methodology, Int. J. Adv. Manuf. Technol. 70(2014), 559-571.

[35] T.L. Schmitz, K.S. Smith, Machining dynamics, frequency response to improved productivity, Springer,2009.

[36] E.E Ungar, Damping of flexural vibrations by alternate viscoelastic and elastic layers, WALIM Technical Report (1959) :59-509.

[37] S.H. Zhang, H.L Chen, A study on the damping characteristics of jaminated composites with integral viscoelastic layers, Compos. Struct. 74 (2006): 63-69.

[38] Y.J. Ji, X.B. Wang, Z.B. Liu, H.J. Wang, L. Jiao, L. Zhang, T. Huang, Milling stability prediction with simultaneously considering the multiple factors coupling effects - regenerative effect, mode coupling, and process damping, In. J. Adv. Manuf. Technol. 97(2018): 2509-27.

[39] S.T. Xi, H.R. Cao, X.F. Chen, Dynamic modeling of spindle bearing system and vibration response investigation, Mech. Syst. Signal Process. 114 (2019): 486-511.

[40] Y. Altintas, Manufacturing automation, metal cutting mechanics, machine tool vibrations and CNC design, 2nd ed. New York: Cambridge University, 2012.

[41] Z. Zhang, H.G. Li, G. Meng, X.T. Tu, C.M. Cheng, Chatter detection in milling process based on the energy entropy of VMD and WPD, Int. J. Mach. Tools Manuf. 108 (2016): 106-12.

[42] J.P. Davim, P. Reis, C. C. António, A study on milling of glass fiber reinforced plastics manufactured by hand-lay up using statistical analysis (ANOVA), Compos. Struct. 64 (2004): 493-500.